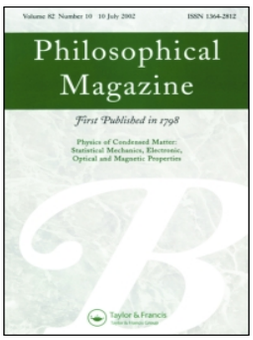

Taylor & Francis
Taylor & Francis Group

Philosophical Magazine B

ISSN: 1364-2812 (Print) 1463-6417 (Online) Journal homepage: https://www.tandfonline.com/loi/tphb20

Complex alloy phases for binary hard-disc mixtures

C. N. Likos & C. L. Henley

To cite this article: C. N. Likos & C. L. Henley (1993) Complex alloy phases for binary hard-disc mixtures, Philosophical Magazine B, 68:1, 85-113, DOI: 10.1080/13642819308215284

To link to this article: https://doi.org/10.1080/13642819308215284

PHILOSOPHICAL MAGAZINE B, 1993, VOL. 68, NO. 1, 85–113

Complex alloy phases for binary hard-disc mixtures

By C. N. LIKOS and C. L. HENLEY

Laboratory of Atomic and Solid State Physics and Materials Science Center, Cornell University, Ithaca, New York 14853-2501, USA

[*Received 11 December 1992 and accepted 5 March 1993*]

ABSTRACT

We investigate the phase diagram of two-dimensional binary mixtures of hard discs. There are two parameters in the problem, the ratio r of the radii of the two discs, and the concentration p of small discs. We determine the possible phases by trying different periodic structures and minimizing the area per particle of the alloy for given r and p. We discover over ten distinct pure phases, along with large regions of the phase diagram which are occupied by 'lattice gas' and 'random tiling' phases. The system tends to separate into two coexisting triangular lattices for $r \gtrsim 0{\cdot}5$. The phase diagram becomes increasingly complicated at small size ratio and large concentrations of small discs.

§ 1. INTRODUCTION

The problem of packing of identical hard spheres is a well studied one. This question is of interest in many fields; in physics, the hard spheres may sometimes model atoms, and their packing arrangements can simulate atomic models of liquids and solids. Less is known about packing properties of mixtures of spheres or discs of two different sizes.

Our system is motivated by the fact that many binary intermetallic phase diagrams are complicated, possessing as many as ten distinct phases at different stoichiometries. Hard spheres model atoms in simple metals to some extent, in that there are no strong constraints on which species may be nearest neighbours to other species (in contrast to ionic crystals), nor on the coordination number (in contrast to molecular crystals).

At the least, sphere packings are a good guide to the ground states of atoms interacting with short-range potentials with sharp wells, such as a truncated Lennard-Jones (L-J) potential. Indeed, we will find (see § 4) that the best binary sphere packings occur when the size ratio takes on magic values, those which allow all neighbouring pairs to be in contact. Manifestly, the ground states for the truncated-potential system will have exactly the same property. (Note that the L-J radii appropriate to a given system need not be additive, but it is plausible that they are in situations where there is little charge transfer; in that case the difference in L-J radii is determined by the size of the cores.)

However, in a real metal, the ideal interatomic radii are not particularly correlated with the ionic sizes; indeed, in alkali metals the ionic sizes are completely irrelevant in determining the lattice constants, and only for the noble metals is the nearest neighbour distance largely determined by the ionic sizes (Ashcroft and Mermin 1976)†.

† For a detailed discussion on the important terms in the Hamiltonian of a metal, see Ashcroft (1982).

Interactions with more distant neighbours are present, mediated through conduction electrons, and the effective potential may include important terms involving three or four atoms.

Still, size ratios are invoked at some times as the determining factor in the placement of the different species within a structure, or in the stability of structure with respect to a competing one. If it is postulated that size ratios are essential in stabilizing a particular structure, then obviously the hard sphere system is the one in which size ratio is the most important; by considering this extreme case, we can better understand how sensitive the phase diagram might be to small changes in the size ratio. At the same time, the hard sphere system has the simplicity of being the only binary mixture system which can be described by *just* two parameters. If size ratios can produce a rich phase diagram in hard-sphere systems, then they are plausible candidates for the factor producing richness in real binary systems. In any case, the hard-sphere system is the simplest model we can study, in order to discover how rich the phase diagram of a two-component intermetallic alloy might be generically.†

The experimental interest is mostly in random, amorphous packing (Quickenden and Tan 1974, Dodds 1975, Bideau, Gervois, Oger, and Troadec 1986) or else in the steady-state configurations produced in non-equilibrium flow or deposition processes. Nevertheless, knowledge of the stable disc packings is probably a useful guide to the nature of local order in good amorphous packings, or to the possible periodic attractors in a deposition model.

In this paper, we study the periodic arrangements of discs of two different sizes, varying both the ratio of their radii and the concentration of the system in one of the components. There are two parameters in the problem: the ratio of the radii

$$r \equiv \frac{r_B}{r_A}, \qquad (r \leqslant 1), \tag{1}$$

and the concentration of the small discs

$$p \equiv \frac{N_B}{N_A + N_B}, \tag{2}$$

where r_A and r_B are the radii of large and small discs, and N_A and N_B the numbers of large and small discs respectively. Without loss of generality, we can set $r_A = 1$. The packing fraction η is defined as the ratio of the volume occupied by the discs over the total volume of the system. We choose to study the two-dimensional problem because of its relative simplicity, and because it offers us the possibility of studying a wide variety of periodic arrangements.

We consider various candidate structures for each value of the size ratio and the concentration, and then apply the space-filling principle to determine which one is the most preferable. For a monodispersed system of hard discs, the arrangement with the highest packing fraction is the triangular close-packed (fig. 1), and the corresponding value of the packing fraction is $\eta = \pi/(12)^{1/2}$. For a system consisting of two kinds of hard discs, there is always the possibility of phase separation into two close-packed

† The structure of intermetallic alloys has been simulated by discs of two sizes in a two-dimensional simplification by Nowick and Mader (1965), and by computation for random sphere packings in two and three dimensions by Visscher and Bolsterli (1972), and many after them.

Fig. 1

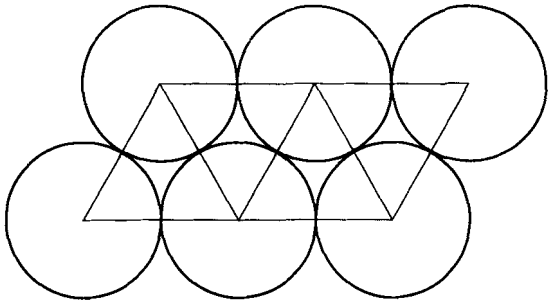

The triangular closed-packed lattice has the lowest volume per atom for a monodispersed system of hard discs.

triangular lattices. However, as the size ratio decreases, we can occupy interstitial sites of the lattice of the large discs with one or more small discs, thus increasing the packing fraction. Other options, such as deforming the lattice of the large discs in order to accommodate small ones, are also available. Our goal here is not to construct a mathematical proof that these structures are optimal, but rather to explore the possibilities of different structures.

In § 2, we briefly review previous results obtained from the study of binary systems of hard spheres and discs. In § 3, we present our model in detail and describe the strategy of guessing various candidate structures. In § 4 we determine the structures with the highest packing fraction as a function of r for a chosen set of number ratios p. In § 5, we construct the phase diagram, and discuss its features. In § 6, we discuss the effects of entropy, the relation of this work to studies in three dimensions, and the relevance of this work to quasicrystals. We conclude in §7.

§ 2. Prior results

2.1. *Freezing of binary mixtures of hard spheres*

Recently, a considerable amount of work was done, both experimentally and theoretically, to study the freezing of a binary mixture of hard spheres. Although the structures formed at freezing are not close-packed, because the spheres are not touching, it seems reasonable to expect that similar structures will be important to both problems of freezing and packing.

The freezing phase transition in a binary suspension of colloidal hard spheres was studied recently by light scattering, neutron scattering, and scanning electron microscopy (Bartlett 1990, Bartlett, Ottewill and Pusey 1990, 1992, Bartlett and Ottewill 1991). Results were obtained for hard spheres of diameter ratio $r = 0{\cdot}61, 0{\cdot}65$ and $0{\cdot}85$. It was found that the fluid phase is stable up to a higher density in the binary mixture system than in the monodisperse system. For the case of diameter ratio $r = 0{\cdot}61$, it was found that the symmetry of the frozen phase depends significantly on the number fraction of the larger component.

Theoretical results on this problem are also available. Thermodynamic phase diagrams for binary mixtures have recently been constructed (Rick and Haymet 1989, Denton and Ashcroft 1990, Zeng and Oxtoby 1990). The first-order freezing transition is treated by different varieties of density functional theory of freezing. Rick and Haymet considered the freezing of hard sphere mixtures of equal number fraction, and they concluded that the stable solid phase at all size ratios is the substitutionally

disordered f.c.c. structure. This is a structure where the two species of atoms occupy the sites of a regular f.c.c. lattice at random. Metastable solutions for different crystal symmetries were also found.

Denton and Ashcroft applied the modified weighted density approximation (MWDA) to study mixtures of various size ratios, for the whole range of concentrations. Several different structures were considered, namely the substitutionally disordered f.c.c. structure, the CsCl, NaCl and zinc-blende structures, and a 'sublattice-melt' structure, in which the larger atoms are localized about the sites of an f.c.c. lattice, while the smaller ones are in a uniform-fluid state. The phase diagram is predicted to evolve from a spindle type in the range $0{\cdot}94 < r < 1$ to an azeotropic type in the range $0{\cdot}87 < r < 0{\cdot}94$, and finally to a eutectic type for $r < 0{\cdot}87$. The disordered f.c.c. structure was found to be the most stable one in the range $0{\cdot}76 < r < 1$. For $r < 0{\cdot}76$, the two phases were found to be immiscible in the disordered f.c.c. solid, and the most stable structure in this region is found to be a *pure* f.c.c. solid composed entirely of large spheres. This finding is consistent with the results of the experimental study by Bartlett *et al.* However, it differs considerably from the predictions of Rick and Haymet who found the disordered f.c.c. solid to be the stable structure at all size ratios. The other structures considered were found to be either metastable for lower values of the size ratio (CsCl, NaCl, 'sublattice-melt) or always mechanically unstable (zinc-blende).

Zeng and Oxtoby used the effective liquid free energy model (ELFEM) to examine the freezing of a binary hard sphere mixture into a substitutionally disordered f.c.c. solid only. Their predictions are in general agreement with the ones from the MWDA. In particular, the find that for $0{\cdot}93 < r < 1$, the phase diagram is spindle-type, and the two types of spheres are found to be completely miscible over the entire range of concentrations. For $0{\cdot}88 < r < 0{\cdot}93$ the phase diagram is azeotrope-type, but the two kinds of spheres are still completely miscible in the solid phase. For the whole region $r < 0{\cdot}88$ the phase diagram is of eutectic type. In the region $0{\cdot}83 < r < 0{\cdot}88$, the f.c.c. solid tends to separate. For diameter ratios $r < 0{\cdot}83$, stable solutions for the substitutionally disordered f.c.c. solid could no longer be found for the whole range of concentrations.

2.2. *Three-dimensional theoretical results*

The effect of the relative ionic sizes in the formation of crystal structures has been examined in the context of the properties of alkali halogenides (Pauling 1960). Pauling presents a detailed discussion on the effect of the relative ionic sizes on properties of the alkali halogenides. It is important to emphasize, however, that ionic systems are characterized by strong long-range Coulomb interactions rather than short-range ones. Therefore, the effect of the size ratio is not one of pure geometrical nature, but rather a combined effect of geometrical configuration and interactions between the ions.

The formation of long-ranged structures in binary hard sphere systems has been observed in some natural gem opals (Sanders 1980). These observations motivated a theoretical effort, in which the space-filling characteristics of the observed structures were studied in more detail (Murray and Sanders 1980). The question addressed was how binary systems of hard spheres might order for any value of the size ratio r of the radii of the two spheres and for any specific concentration of large spheres, and whether or not this ordering is governed solely by the principle of maximization of the packing fraction η. It was found that a mixture of the hexagonal phase AB_2 with the cubic phase AB_{13} is stable in the region $0{\cdot}558 < r < 0{\cdot}570$. Below $r = 0{\cdot}458$ a phase AB of the NaCl type is formed, and as both the concentration of the large (A) spheres and size ratio

decrease, other structures become possible because more small (B) spheres can be accommodated in a close-packed A sublattice. In the region $0{\cdot}624 < r < 1$, A and B segregate into two close-packed monodispersed phases. Finally, AB_2 is likely to exist in equilibrium with monodispersed A or B depending on the concentration, for $0{\cdot}482 < r < 0{\cdot}550$ and $0{\cdot}550 < r < 0{\cdot}624$. We emphasize that this work is the most similar to ours; however, our calculations were made for a two-dimensional binary system, which offered us the opportunity of studying a larger variety of candidate structures.

A somewhat different approach to the packing problem is one where the packing is defined *locally* rather than globally (Szeto and Villain 1987, Villain, Szeto, Minchau and Renz 1988). In this context, a packing of hard spheres is called dense if the space is filled with tetrahedra formed by mutually touching nearest neighbours. If only one species of hard spheres is considered, dense packings of regular tetrahedra do not exist because the dihedral angle of a regular tetrahedron $\gamma_0 = 70{\cdot}5°$ is not a multiple of 2π. However, the gaps or defects found in the packing of regular tetrahedra can be avoided if we introduce a second species of atoms. A simple example of such structures is the NaCl structure. A whole set of more complicated solutions can also be found.

2.3. *Two-dimensional theoretical results*

A detailed discussion of the problem of packing of hard discs is given by Fejes Tóth (1964, 1972). The problem is stated as follows: suppose that we have an inexhaustible stockpile of all kinds of hard discs, the radii of which lie in a given interval (a, b). How must the discs be chosen and arranged in order to fill the Euclidean plane as densely as possible? A variety of packings is discovered, and the dependence of the packing fraction upon the size ratio and the concentrations is discussed. Some of the packings require discs to be chosen from *two* different species; others require more kinds of discs. We will discuss the packings that are relevant to our work in the § 4, in the context of our exploration of the phase diagram.

§ 3. The model

3.1. *Definition of the problem*

We consider a system consisting of hard discs of two different sizes, large (A) and small (B). The size ratio r and the concentration p of small discs are defined in eqns. (1) and (2) respectively. In a hard-sphere system, the important thermodynamic variable is the density, or its conjugate variable, the pressure P.

We assume that our system is in contact with a much larger system which acts on it as a 'pressure bath', i.e. it exerts a constant pressure P on it. Since for any hard-sphere system there are no interparticle interactions, the Hamiltonian is

$$H = PV, \tag{3}$$

where V is the two-dimensional volume V (area) occupied by the system. Without loss of generality, we take $P \equiv 1$. We are interested here in the limit $T \to 0$, so we will ignore the contributions to the free energy from entropy in our calculation.

We proceed as follows: the first stage is to construct various candidate structures. Here, a 'structure' (or a 'phase') can be defined by specifying which atoms are in hard contact with which others, so that a 'structure' may be defined over a range of radius ratios r even though the interatomic bond angles and the shape of the unit cell may be changing. For each phase s, one can define a volume per atom $v_s(r)$, as well as a number ratio p_s.

Fig. 2

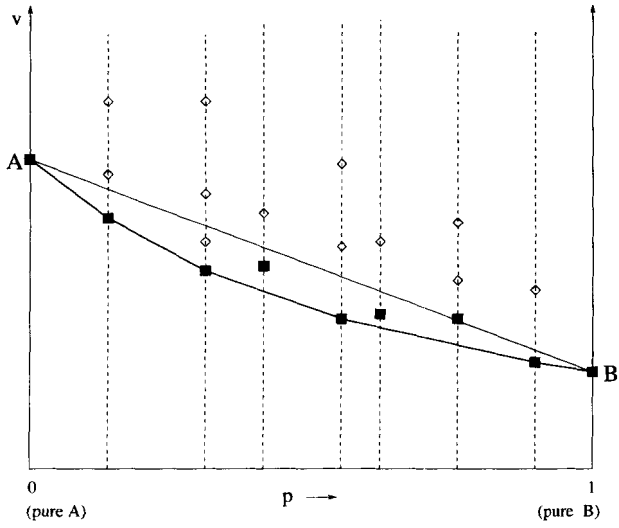

Method of constructing the volume per atom v against number ratio p curve for a given value of diameter ratio r. The ■-symbols on the vertical dotted lines represent the volume per atom for the structure with the highest packing fraction for the specific concentration. The ◇-symbols represent the volume per atom of other candidate structures which have lower packing fractions, and thus they are not considered in the construction of the v against p curve. Notice that the curve has to be concave up, thus its construction *does not* amount to simply connecting the ■-symbols.

Physically, for a given number fraction p, the minimum volume is often achieved by a coexistence of two phases s and s', each of course having the same given r, and including number fractions n and $n' = 1 - n$ of all the atoms. In that case, the net volume per atom is

$$v = nv_s(r) + n'v_{s'}(r), \tag{4a}$$

and the overall number fraction is

$$p = np_s(r) + n'p_{s'}(r). \tag{4b}$$

This optimization is simply expressed graphically in the (p, v) plane: we simply connect the point $(p_s(r), v_s(r))$ to the point $(p_{s'}(r), v_{s'}(r))$ by a straight line segment. The optimal $v(p, r)$ (for the given r) is then given by taking the minimum of all such line segments at each p. (We will refer to this as the 'surviving' phase.)

Note that if phase s has a volume greater than that of $A + B$ coexistence, then it lies above the chord 'AB' in fig. 2, and the segment representing s–s' coexistence is always above the one representing A–s' or B–s' coexistence (depending on whether $p_{s'} > p_s$ or $p_{s'} < p_s$, respectively). Thus such phases never need be considered. For convenience, as soon as we determine $v_s(r)$ for a given phase, we compare this with the volume of a coexisting mixture of the one-component A and B triangular phases, namely

$$v_{A+B}(r) \equiv (1-p)(2\sqrt{3}) + p(2\sqrt{3r^2}). \tag{5}$$

This way, we eliminate phases s from further consideration for the values of r at which $v_s(r) > v_{A+B}(r)$.

Also, we often find more than one candidate phase at the same number ratio, i.e. $p_s = p_t$, with $v_s(r) < v_t(r)$. In such a case, the line segment from (p_s, v_s) to $(p_{s'}, v_{s'})$ is lower everywhere than the segment from (p_s, v_t) to $(p_{s'}, v_{s'})$; this coexistence with phase t can never be optimal, and we need not consider it when performing the graphical construction of fig. 2. Therefore, before constructing the whole curve $v(p; r)$, we first make comparisons among the pure phases s with the same p_s, and keep only the one with minimum v_s for further consideration. This reduces the number of comparisons that must be made at the next step. On fig. 2, the higher volume phases are marked with open diamonds and the minimum volume phase is marked by the filled squares.

Finally, the volume per atom for a given r and for any value of p is determined by connecting the points for the chosen set by straight segments, but in such a way that the resulting curve is everywhere concave up (see fig. 2). Thus, the straight segments in fig. 2 represent the volume per atom of the coexistence between the structures represented by their endpoints. This procedure is carried out in § 5.

3.2. *Systematics of guessing structures*

For a monodispersed system of hard discs, the highest packing is achieved by the triangular lattice. Filling the interstices of such a lattice consisting of large discs with small ones, increases the packing fraction. Whatever the configuration of the large discs might be (triangular, square, hexagonal etc.), there are 'magic' ratios, i.e. specific values of the size ratio for which one small disc fits exactly into the interstices of the lattice formed by the large discs. When the size ratio is different from these 'magic' values, it is necessary to apply a shear in the lattice in order to achieve mechanical stability, meaning that all the nearest neighbours are in close contact. Also, substituting one small disc by two (or more) in a close-packed structure, or a large disc by a cluster of small ones might lead to another close packed structure with a higher concentration. Finally, we can combine the unit cell of one structure with one or more unit cells of another structure, thus creating a new unit cell for a different periodic structure, whenever that is possible. This way, we generate a 'random tiling' of the plane. Thus, the four major techniques used here for guessing structures are:

(i) filling interstices with small discs,
(ii) replacing one disc by several smaller discs,
(iii) shearing the lattice, and
(iv) combining the unit cells of different structures.

We now proceed to examine the various candidate structures.

§ 4. Candidate structures

In this § we consider candidate structures for a chosen set of number fractions p. We wish to choose the structures which minimize the volume per atom, $v(r, p)$. We consider a set of (simple rational) p values. For each p, we consider one or more periodic (single-phase) structures. In order to eliminate the hopeless ones, we compare $v(r, p)$ among our structures, and also compare with the volume per atom of the $A + B$ coexistence for every value of r, as explained in § 3.1. Thus, for every r, we end up with a 'winning' set of structures at various rational p's. In the process, we discover two kinds of phases, the 'pure' phases and the 'random' phases.

The pure phases exist for mixtures of a specific concentration only. Furthermore, there are special values of the radius ratio, where a kind of 'optimal' packing occurs, i.e. any disc (small or large) is in hard contact with all its immediate neighbours. In other

words, the A–A pairs are at distance $2r_A$, the A–B pairs are at distance $r_A + r_B$, etc. We call such values of r 'magic'. Usually, a pure phase is generated by first finding the 'magic' value of r, and then, for different values of r, by distorting the unit cell of the structure.

On the other hand, the random phases exist for mixtures of variable concentrations, and fall into two subcategories, the 'lattice-gas' and 'random-tiling' phases. The former are characterized by the property that small discs, or clusters of small discs occupy at random any of the available interstitial sites of the pure A triangular lattice (see § 4.8). The latter are built out of space-filling packings of the unit cells of different pure structures (technique (iv) above), but this combination occurs in a random rather than in a periodic fashion (see § 4.9).

The rest of this § is organized as follows: first, we study mixtures having the particular concentrations for which the pure phases exist. Then, we discuss the two kinds of random phases, and finally we speculate about a region of the phase diagram

Table 1. The various alloy phases with the range of diameter ratios, the Bravais symmetry, and the figure where the unit cell is shown. The double horizontal lines separate the pure from the 'lattice-gas' phases, and the 'lattice-gas' from the 'random tiling' phases. For the random phases, we show all the possible local environments for the A and B discs.

Phase	Condition (A discs)	Condition (B discs)	Radius	Bravais symmetry	Fig.
$T_1(AB_2)$	A:6A	B:ø	$(0, r_1)$	Hexagonal	
	A:6A+6B	B:3A	$r_1 = 0{\cdot}155$	Hexagonal	3
	A:4A+6B	B:3A	(r_1, r_2)	Cent. rectangular	4(*a*)
	A:4A+6B	B:3A+B	$r_2 = 0{\cdot}281$	Cent. rectangular	4(*b*)
	A:6B	B:3A+B	$(r_2, 1)$	Cent. rectangular	4(*c*)
$H_1(AB_2)$	A:2A+6B	B:3A	(r_1, r_3)	Cent. rectangular	5(*b*)
	A:2A+6B	B:3A+2B	$r_3 = 0{\cdot}533$	Cent. rectangular	5(*a*)
	A:6B	B:3A+2B	$(r_3, 1)$	Cent. rectangular	5(*c*)
$S_1(AB)$	A:4A+3B	B:3A	(r_1, r_4)	Cent. rectangular	6(*b*)
	A:4A+4B	B:4A	$r_4 = 0{\cdot}414$	Square	6(*a*)
	A:2A+4B	B:4A	$(r_4, 1)$	Rectangular	7(*a*)
$H_2(AB)$	A:3A+4B	B:4A	(r_4, r_5)	Cent. rectangular	7(*b*)
	A:3A+4B	B:4A+B	$r_5 = 0{\cdot}637$	Cent. rectangular	8(*a*)
	A:2A+4B	B:4A+B	$(r_5, 1)$	Cent. rectangular	8(*b*)
$T_2(AB_6)$	A:6A	B:ø	$(0, r_6)$	Hexagonal	
	A:6A+12B	B:2A+2B	$r_6 = 0{\cdot}101$	Hexagonal	9(*b*)
	A:12B	B:2A+2B	(r_6, r_7)	Hexagonal	9(*b*)
	A:12B	B:2A+3B	$r_7 = 0{\cdot}349$	Hexagonal	10
	A:ø	B:3B	$(r_7, 1)$	Hexagonal	
$S_2(AB_4)$	A:4A+8B	B:2A+B	(r_6, r_8)	Cent. rectangular	11(*b*)
	A:4A+8B	B:2A+2B	$r_8 = 0{\cdot}216$	Square	11(*a*)
	A:8B	B:2A+2B	(r_8, r_9)	Square	12(*a*)
	A:8B	B:2A+3B	$r_9 = 0{\cdot}620$	Square	12(*b*)
$H_3(A_2B_7)$	A:3A+4B	B_1:2A+B			
		B_2:ø	(r_6, r_{10})	Monoclinic	14
	A:3A+6B	B_1:6B			
		B_2:2A+2B	$r_{10} = 0{\cdot}386$	Hexagonal	13(*a*)
	A:6B	B_1:6B			
		B_2:2A+2B	$(r_{10}, 1)$	Hexagonal	13(*b*)

Table 1. *continued*

Phase	Condition (A discs)	Condition (B discs)	Radius	Bravais symmetry	Fig.
$T_3(AB_8)$	$A:6A$	$B:\text{ø}$	$(0,r_{11})$	Hexagonal	
	$A:6A+12B$	$B_1:2A+B$			
		$B_2:3B$	$r_{11}=0{\cdot}082$	Hexagonal	15
	$A:12B$	$B_1:2A+B$			
		$B_2:3B$	(r_{11},r_{12})	Hexagonal	16(a)
	$A:12B$	$B_1:2A+2B$			
		$B_2:3B$	$r_{12}=0{\cdot}233$	Hexagonal	16(b)
$T_1^*(AB_{2-\delta})$	$A:6A$	$B:\text{ø}$	$(0,r_1)$	(Hexagonal)[a]	
	$A:6A+xB$	$B:3A$	$r_1=0{\cdot}155$	(Hexagonal)[a]	17($\delta=1$)
	$(0\leqslant x\leqslant 6)$				18($\delta=\frac{3}{2}$)
$T_2^*(AB_{6-\delta})$	$A:6A$	$B:\text{ø}$	$(0,r_6)$	(Hexagonal)[a]	19($\delta=2$)
					20($\delta=\frac{5}{2}$)
	$A:6A+xB$	$B:2A+B$	$r_6=0{\cdot}101$	(Hexagonal)[a]	
	$(0\leqslant x\leqslant 12)$	$2A+2B$			
		ø			
$RT[(AB_2)_x,(A)_y]$	$A:4A+6B$	$B:3A$	(r_1,r_2)	(Incommensurate)[a]	21(a)($y/x=1$)
	$6A$			($D=4$)	22($y/x=3$)
	$5A+3B$				
	$A:4A+6B$	$B:3A+B$	$r_2=0{\cdot}281$	(Incommensurate)[a]	
	$6A$			($D=4$)	
	$5A+3B$				
	$A:6B$	$B:3A+B$	$(r_2,1)$	(Incommensurate)[a]	21(b)($y/x=1$)
	$4A$			($D=3$)	
	$2A+3B$				
$RT[(AB)_x,(A)_y]$	$A:5A+B$	$B:3A$	(r_1,r_4)	(Incommensurate)[a]	23(a)($y/x=1$)
	$5A+2B$			($D=4$)	
	$4A+3B$				
	$4A+4B$				
	$6A$				
	$A:5A+2B$	$B:4A$	$r_4=0{\cdot}414$	(Incommensurate)[a,b]	
	$4A+4B$			($D=4$)	
	$6A$				
	$A:2A+4B$	$B:3A$	$(r_4,1)$	(Incommensurate)[a]	23(b)($y/x=1$)
	$4A+2B$			($D=3$)	
	$6A$				

[a] The symmetry shown refers to an ensemble-average structure. The examples in figs. 17–23 are all monoclinic.

[b] For the special case $y/x=2/\sqrt{3}$, the ensemble average has dodecagonal symmetry (see § 6.3).

which has not been systematically explored. The results are summarized in tables 1 and 2. Table 1 shows the phases discovered, the number of discs that are in hard contact with a large (A) or small (B) disc in each one, and the underlying Bravais symmetry. Table 2 shows the intervals of r for which each phase (pure or random) *can* exist, the specific volume of each phase, and, finally, the intervals of r in which each phase 'wins' the competition among all the various phases at the *same* value of p only (including the $A+B$ coexistence). Thus, in connection with fig. 2, for any given value of r, the phase for which this value lies in its 'winning' interval will be represented by a filled square, and the other ones with the same concentration by the open diamonds.

4.1. AB_2 *mixture* ($p = 2/3$)

This mixture offers a good starting point because, if r is sufficiently small, we can form a periodic structure by putting one small disc in every interstice of a pure triangular A lattice. We call this phase T_1. Clearly, there is a critical radius r_1 of the small discs, for which the small discs fit exactly into the interstices, as shown in fig. 3. This 'magic' radius is

$$r_1 = \frac{2\sqrt{3}}{3} - 1 = 0{\cdot}155. \tag{6}$$

When r increases beyond the value r_1, we distort the triangular lattice so that it can still accommodate two small discs per unit cell, as shown in fig. 4 (*a*). Yet, there is another 'magic' radius r_2, for which *two* small discs fit neatly into the space between large discs in this distorted lattice, as shown in fig. 4 (*b*). This 'magic' radius is

$$r_2 = \frac{-3 + (17)^{1/2}}{4} = 0{\cdot}281. \tag{7}$$

If, now, r becomes larger than r_2, the large discs will lose contact with one another, but they will still be in contact with the small ones, as shown in fig. 4 (*c*). This unit cell can be repeated to fill all space, all the way up to $r = 1$.

Table 2. The specific volume of the various alloy phases. The specific volume of the $A + B$ coexistence is also shown for comparison. The fourth column shows the interval of r in which each of the phases has the lowest volume per atom, compared with the rest of the phases for the same value of p. The double horizontal lines separate mixtures of different concentration of B discs.

Phase	Radius	Volume per atom	'Winning' interval
$T_1(AB_2)$	$[0, r_1]$ $(r_1, r_2]$ $(r_2, 1]$	$2\sqrt{3}/3$ $8(r^2+2r)^{1/2}/[3(1+r)^2]$ $2(1+2r)^{3/2}/3$	$[0, 0{\cdot}312]$
$H_1(AB_2)$	$(r_1, r_3]$ $(r_3, 1]$	$2[(r^2+2r)^{1/2}+1+r]/3$ $8r(1+2r)^{3/2}/[3(1+r)^2]$	$[0{\cdot}517, 0{\cdot}546]$
$A + B(AB_2)$	$[0, 1]$	$2\sqrt{3}(1+2r^2)/3$	$(0{\cdot}312, 0{\cdot}517) \cup (0{\cdot}546, 1]$
$T_1^*(AB_{2-\delta}); \delta = 1$	$[0, r_1]$	$\sqrt{3}$	$[0, r_1]$
$RT[(AB_2), (A)]$	$(r_1, r_2]$ $(r_2, 1]$	$[8(r^2+2r)^{1/2}/(1+r)^2 + 2\sqrt{3}]/4$ $[(V_1+V_2)/4]^{(a)}$	$(r_1, 0{\cdot}299]$
$S_1(AB)$	$(r_1, r_4]$ $(r_4, 1]$	$4(r^2+2r)^{1/2}/(1+r)^2$ $2(r^2+2r)^{1/2}$	$[0{\cdot}392, r_4]$
$H_2(AB)$	$(r_4, r_5]$ $(r_5, 1]$	$[(3W_1+W_2)/2]^{(b)}$ $[(2X_1+X_2+X_3)/2]^{(c)}$	$(r_4, 0{\cdot}438] \cup [0{\cdot}627, 0{\cdot}646]$
$A + B(AB)$	$[0, 1]$	$\sqrt{3}(1+r^2)$	$(0{\cdot}299, 0{\cdot}392) \cup (0{\cdot}438, 0{\cdot}627) \cup (0{\cdot}646, 1]$
$T_1^*(AB_{2-\delta}); \delta = 3/2$	$[0, r_1]$	$4\sqrt{3}/3$	$[0, r_1]$
$RT[(AB_2), (A)_3]$	$(r_1, r_2]$ $(r_2, 1]$	$[8(r^2+2r)^{1/2}/(1+r)^2 + 6\sqrt{3}]/6$ $[(V_1+3V_2)/6]^{(a)}$	$(r_1, 0{\cdot}291]$
$RT[(AB), (A)]$	$(r_1, r_4]$ $(r_4, 1]$	$[8(r^2+2r)^{1/2}/(1+r)^2 + 2\sqrt{3}]/3$ $[4(r^2+2r)^{1/2} + 2\sqrt{3}]/3$	$[0{\cdot}392, 0{\cdot}436]$
$A + B(A_2B)$	$[0, 1]$	$2\sqrt{3}(2+r^2)/3$	$(0{\cdot}291, 0{\cdot}392) \cup (0{\cdot}436, 1]$

Table 2. *continued*

Phase	Radius	Volume per atom	'Winning' interval
$T_2(AB_6)$	$[0, r_6]$	$2\sqrt{3}/7$	$[0, 0{\cdot}157]\cup[0{\cdot}315, 0{\cdot}354]$
	$(r_6, r_7]$	$(3/7)r(1+2r)^{1/2}+(3\sqrt{3}/14)(1+2r)+(\sqrt{3}/14)r^2$	
	$(r_7, 1]$	$[12r^2\tan(5\pi/12)+2\sqrt{3}r^2]/7$	
$A+B(AB_6)$	$[0, 1]$	$2\sqrt{3}(1+6r^2)/7$	$(0{\cdot}157, 0{\cdot}315)\cup(0{\cdot}354, 1]$
$T_2^*(AB_{6-\delta}); \delta=2$	$[0, r_6]$	$2\sqrt{3}/5$	$[0, r_6]$
$S_2(AB_4)$	$(r_6, r_8]$	$\{[2(1+r)^2\sin\omega\cos\omega+4r(1+r)\sin\omega+4(1+r)\sin\phi+2r(1+r)\cos t]/5\}$[d]	$(r_6, 0{\cdot}123]\cup[0{\cdot}193, 0{\cdot}245]$
	$[r_8, r_9]$	$2[(1+2r)^{1/2}+r]^2/5$	
$A+B(AB_4)$	$[0, 1]$	$2\sqrt{3}(1+4r^2)/5$	$(0{\cdot}123, 0{\cdot}193)\cup(0{\cdot}245, 1]$
$T_2^*(AB_{6-\delta}); \delta=5/2$	$[0, r_6]$	$4\sqrt{3}/9$	$[0, r_6]$
$H_3(A_2B_7)$	(r_6, r_{10})	$[(12\sin\phi\cos\phi+4\sqrt{3}\sin^2\phi)/9]$[e]	$(r_6, 0{\cdot}110]\cup[0{\cdot}378, 0{\cdot}408]$
	$(r_{10}, 1]$	$\sqrt{3}[(1+2r)^{1/2}+\sqrt{3}r]^2/6$	
$A+B(A_2B_7)$	$[0, 1]$	$2\sqrt{3}(2+7r^2)/9$	$(0{\cdot}110, 0{\cdot}378)\cup(0{\cdot}408, 1]$
$T_3(AB_8)$	$[0, r_{11}]$	$2\sqrt{3}/9$	$[0, 0{\cdot}118]$
	$(r_{11}, r_{12}]$	$[2\sqrt{3}/9(1+r)^2\cos^2\phi]$[f]	
$A+B(AB_8)$	$[0, 1]$	$2\sqrt{3}(1+8r^2)/9$	$(0{\cdot}118, 1]$

[a] $V_1=2(1+2r)^{3/2}$;
$V_2=[(1+3r+2r^2)(7-3r-2r^2)]^{1/2}$.

[b] $W_1=(r^2+2r)^{1/2}$;
$W_2=(r^2+2r)^{1/2}(3-2r-r^2)(3r^2+6r-1)/(1+r)^4$.

[c] $X_1=(r^2+2r)^{1/2}$;
$X_2=r(1+2r)^{1/2}$;
$X_3=\{2[(r^2+2r)(1+2r)]^{1/2}-r(r^2+2r-1)\}\times[(r^2+2r-1)(1+2r)^{1/2}+2r(r^2+2r)^{1/2}]/(1+r)^4$.

[d] $\sin\phi=(r^2+2r)^{1/2}/(1+r)$;
$\cos t=(1+2r)^{1/2}/(1+r)$;
$\omega=\pi/2-(2\phi+t)$, (see fig. 11 (*b*)).

[e] $\exp(i\phi)=[(1+2r)^{1/2}+ir][1+i(r^2+2r)^{1/2}]/(1+r)^2$, (see fig. 14).

[f] $\sin t=r\sqrt{3}/(1+r)$;
$\phi+t=\pi/6$, (see fig. 16 (*a*)).

Fig. 3

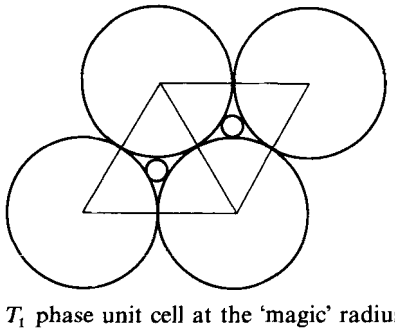

The T_1 phase unit cell at the 'magic' radius r_1.

Fig. 4

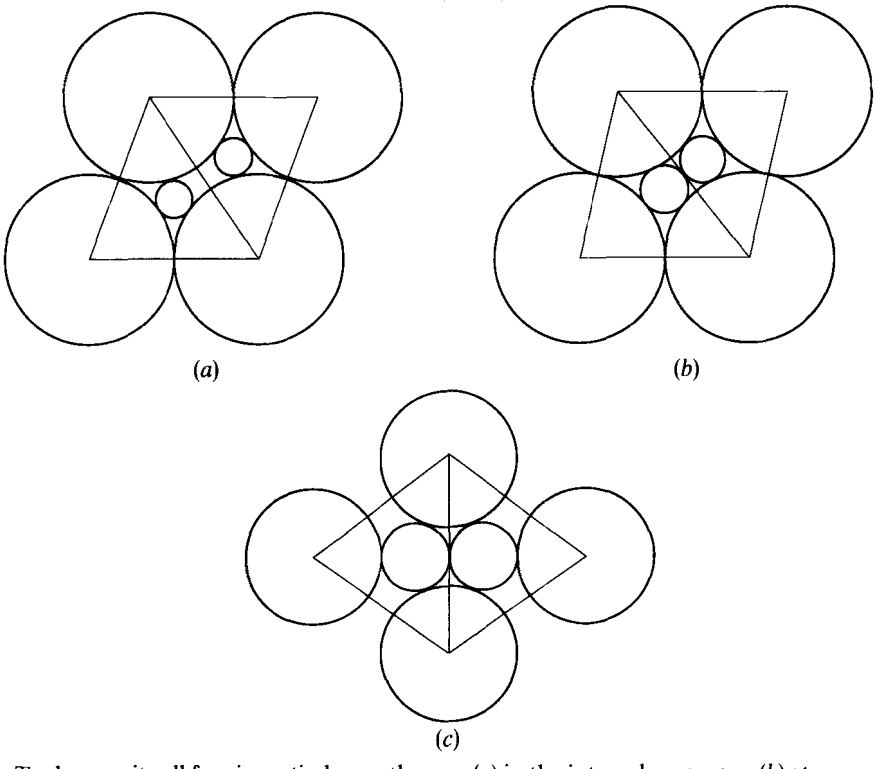

The T_1 phase unit cell for size ratio larger than r_1: (*a*) in the interval $r_1 < r < r_2$. (*b*) at $r = r_2$. (*c*) in the interval $r_2 < r < 1$.

A different way of accommodating small discs in the space between large ones is shown in fig. 5 (*a*). In this case, the new phase, called H_1, has a hexagonal unit cell, which contains three large discs and six small ones. The 'magic' radius for which this configuration occurs is

$$r_3 = 0{\cdot}533. \tag{8}$$

When r becomes smaller than r_3, the small discs lose contact with each other, whereas the large ones still maintain contact, as shown in fig. 5 (*b*). We note that for $r = r_1$, the H_1 phase reduces to the T_1 phase. When r exceeds the value r_3, the *large* discs lose contact, as shown in fig. 5 (*c*).

4.2. AB *mixture* (p = *1/2*)

In the previous subsection, we found the 'magic' radius r_1 for which we can fit one small disc in the interstice formed by the triangular A lattice. For this mixture, there is another magic ratio for which the small discs fit exactly into the interstices of a square A lattice, as shown in fig. 6 (*a*). This magic ratio is

$$r_4 = \sqrt{2} - 1 = 0{\cdot}414. \tag{9}$$

We call the phase with the square unit cell S_1. For values of r larger than r_1 but smaller than r_4, the unit cell will be distorted and will have the shape shown in fig. 6 (*b*). We note that for $r = r_1$ the S_1 phase reduces to a particular realization of the 'lattice-gas' T_1^*

Fig. 5

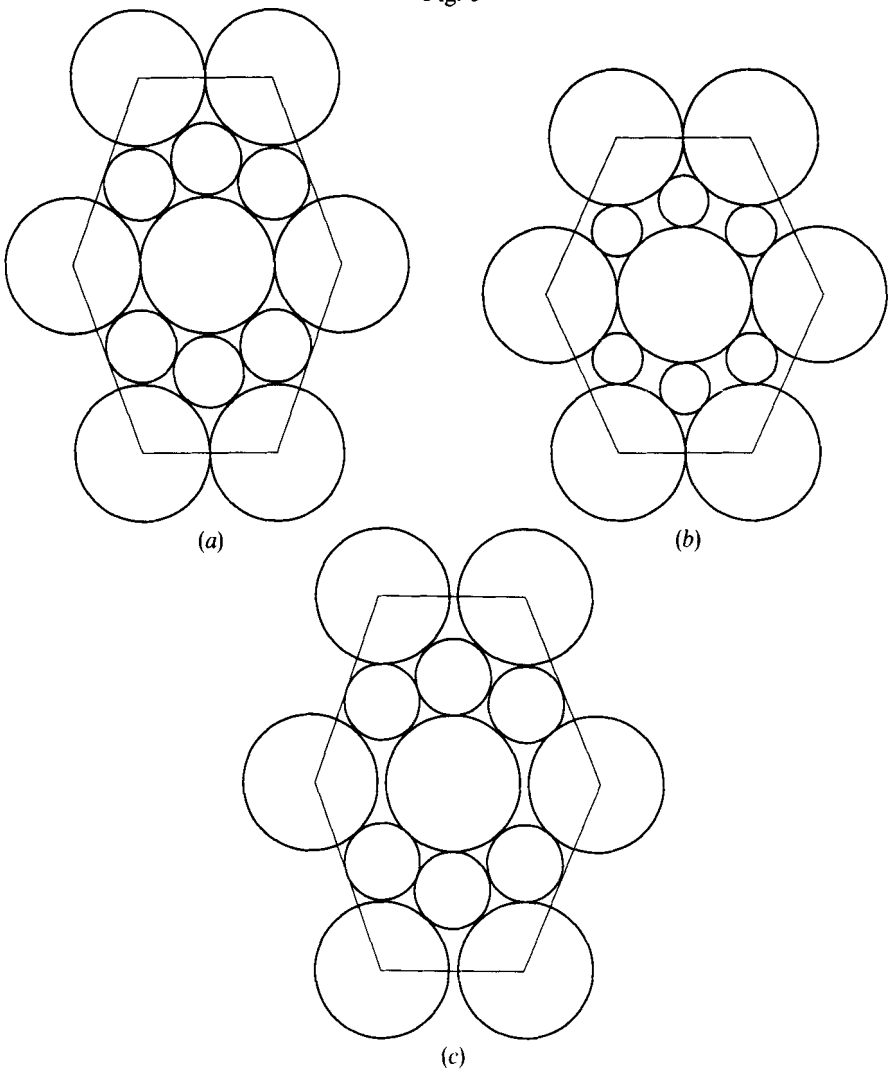

The H_1 phase unit cell for size ratios larger than r_1: (*a*) at $r = r_3$. (*b*) in the interval $r_1 < r < r_3$. (*c*) in the interval $r_3 < r < 1$.

phase (to be described below). When r exceeds the value r_4 there are two ways of deforming the squares in order to accommodate the small discs. We can either stretch them in one direction, thus producing a rectangular unit cell shown in fig. 7 (*a*); or we can joint two adjacent squares together, and make the large discs in the middle lose contact, producing a hexagonal unit cell as shown in fig. 7 (*b*). We still call the phase with the rectangular unit cell S_1, and we name the phase with the hexagonal unit cell H_2. (The Bravais symmetry for this phase is centred rectangular.) On the other hand, as r increases, there will be another magic ratio r_5 for which the small discs of the H_2 phase unit cell will touch, as shown in fig. 8 (*a*). The value is

$$r_5 = 0{\cdot}637. \tag{10}$$

When r increases beyond r_5, the large discs lose contact as shown in fig. 8 (*b*).

Fig. 6

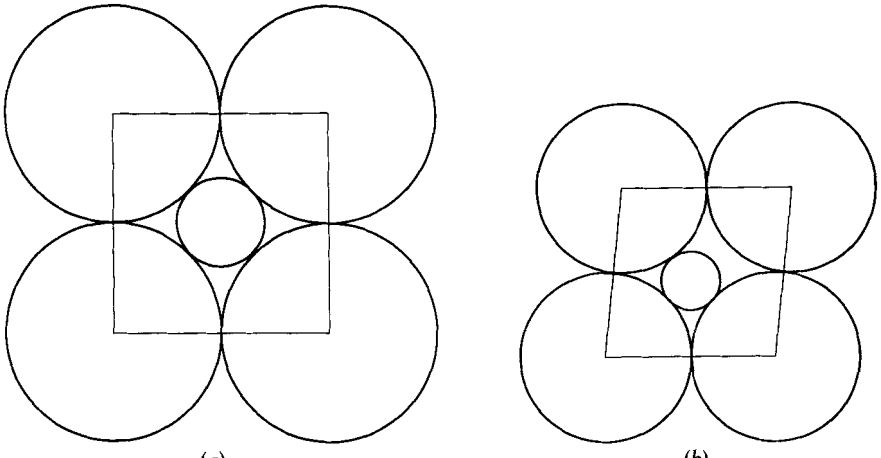

(*a*) (*b*)

The S_1 phase unit cell: (*a*) at $r=r_4$. (*b*) in the interval $r_1<r<r_4$.

Fig. 7

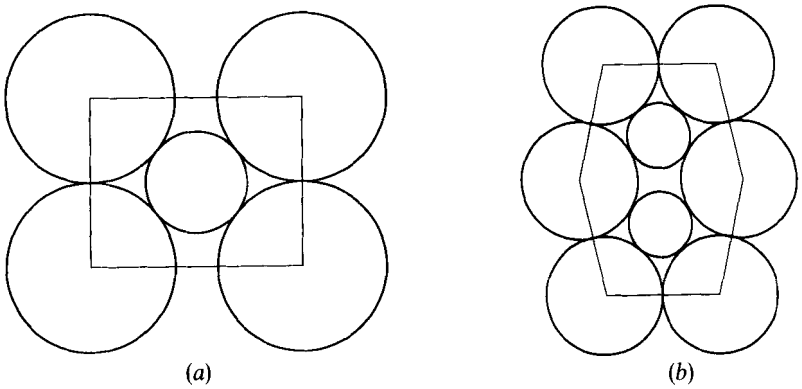

(*a*) (*b*)

(*a*) The S_1 phase unit cell in the interval $r_4<r<1$. (*b*) The H_2 phase unit cell in the interval $r_4<r<r_5$.

Fig. 8

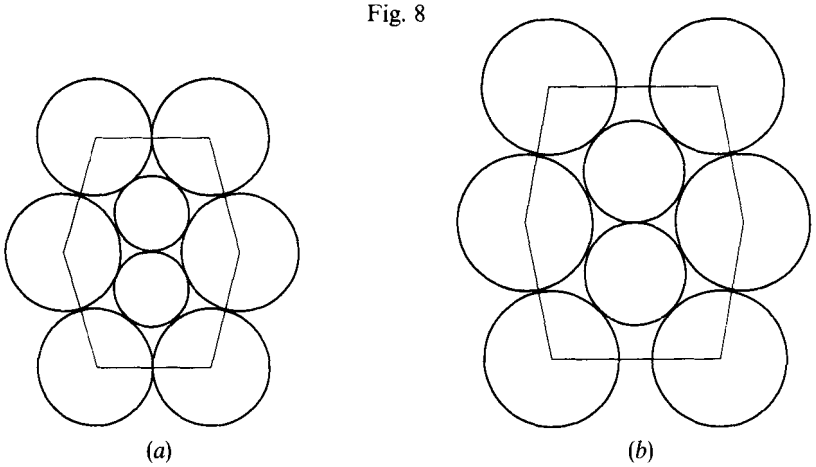

(*a*) (*b*)

The H_2 phase unit cell (*a*) at $r=r_5$. (*b*) in the interval $r_5<r<1$.

4.3. AB_6 *mixture* (p = 6/7)

When the concentration p exceeds the value 2/3, i.e. for mixtures of the form AB_x, with $x > 2$, we find that for r sufficiently small we have to place more than one small disc in the interstitial space if the pure triangular A lattice. Since the open spaces of the triangular lattice have also triangular symmetry (see fig. 1), one is tempted to examine a mixture for which three small discs can be placed there, and this is the AB_6 mixture. As expected, there is again a 'magic' size of the radius of the small discs, for which the three small discs fit nicely into the interstices, as shown in fig. 9 (*a*). We call this phase T_2 phase. The 'magic' radius is

$$r_6 = 5 - 2\sqrt{6} = 0{\cdot}101. \tag{11}$$

When r exceeds the value r_6, we let the unit cell expand uniformly, as shown in fig. 9 (*b*). But this expansion can only continue up to the point where the small discs in adjacent triangles shown in fig. 9 (*b*) come in touch with each other. This will happen when the radius of the small discs takes the 'magic' value

$$r_7 = \frac{\sin(\pi/12)}{1 - \sin(\pi/12)} = 0{\cdot}349. \tag{12}$$

When $r = r_7$, the unit cell will have the shape shown in fig. 10. We can think of this unit cell as being formed by dodecagons with two equilateral B triangles attached at opposite sides. When r exceeds the value r_7, we let the unit cell of the T_2 phase expand uniformly.

4.4. AB_4 *mixture* (p = 4/5)

By analogy with the S_1 phase for the AB mixture, one can form here another phase with square Bravais symmetry, which we call S_2. The unit cell is shown in fig. 11 (*a*), and the 'magic' radius for which this unit cell can be formed is

$$r_8 = 0{\cdot}216. \tag{13}$$

When $r_6 < r < r_8$ we deform the S_2 unit cell by 'squeezing' along one of the diagonals and stretching along the other, thus resulting into the unit cell shown in fig. 11 (*b*). For $r = r_6$ the S_2 phase reduces to a particular realization of the 'lattice-gas' T_2^* phase. On the other hand, when r exceeds the 'magic' value r_8, we let the unit cell of the S_2 phase

Fig. 9

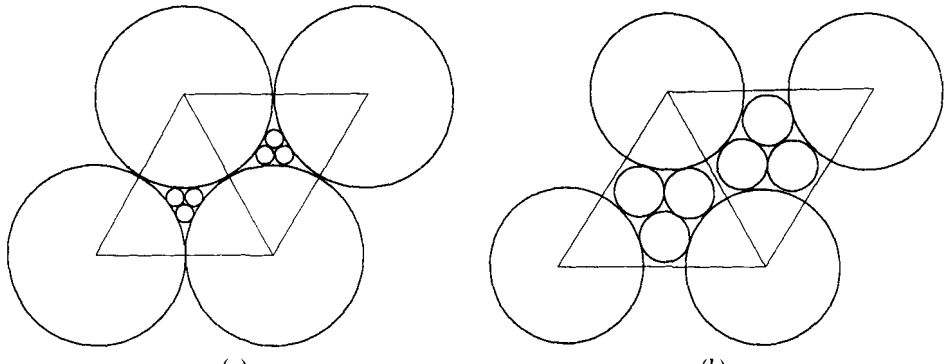

(*a*) (*b*)

The T_2 phase unit cell (*a*) at $r = r_6$ and (*b*) for $r_6 < r < r_7$.

Fig. 10

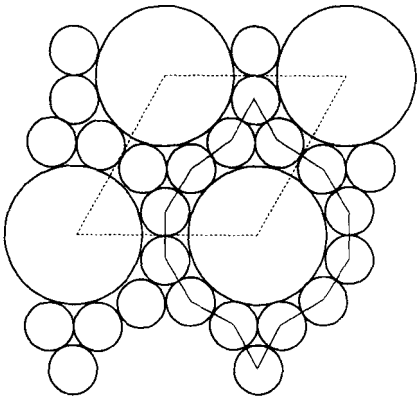

The T_2 phase at the value $r=r_7$. The solid and dotted polygon lines show two alternative shapes of the unit cell.

Fig. 11

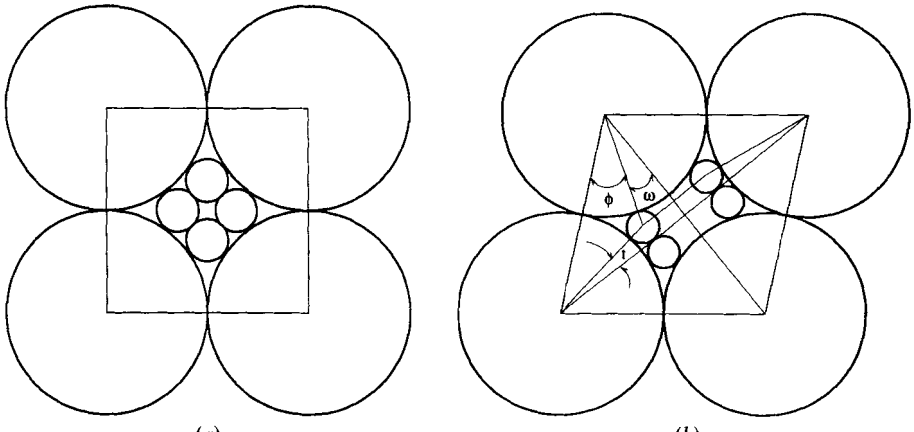

The S_2 phase unit cell: (*a*) for $r=r_8$ and (*b*) for $r_6<r<r_8$.

expand uniformly, as shown in fig. 12(*a*). This can happen until the small discs from adjacent squares touch. This will occur when the radius assumes the 'magic' value r_9

$$r_9=\frac{\sin(\pi/8)}{1-\sin(\pi/8)}=0{\cdot}620. \tag{14}$$

The shape of the unit cell at $r=r_9$ is shown in fig. 12(*b*). It can be thought of as an octagon with a square attached to one of its sides, so we have an octagonal-square tiling of the plane. However, this structure never materializes, i.e. it has packing fraction lower than the $A+B$ coexistence (see table 2).

4.5. A_2B_7 *mixture* (p = 7/9)

The A_2B_7 mixture is another good candidate for exploring the possibility of forming closed-packed periodic structures, because one can form such a structure by replacing one large A disc in the pure triangular A lattice, by a cluster of seven small

Fig. 12

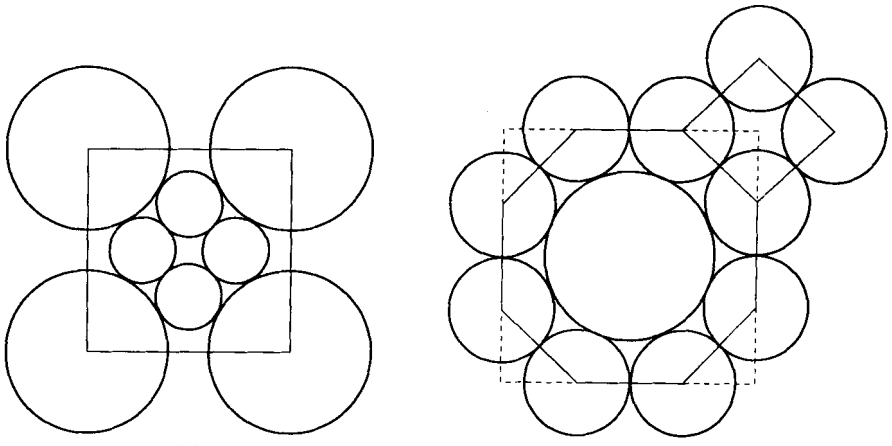

(*a*) (*b*)

The S_2 phase unit cell: (*a*) for $r_8 < r < r_9$ and (*b*) at $r = r_9$. The solid and dotted lines denote two alternative shapes of the unit cell.

Fig. 13

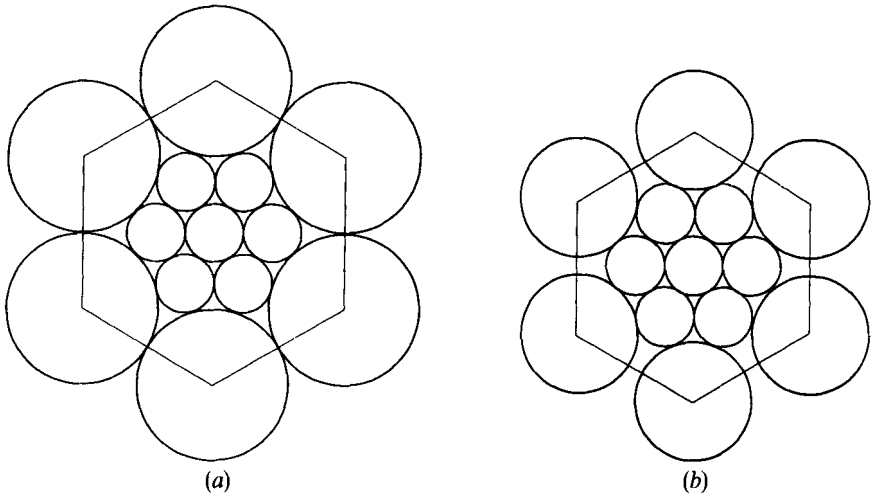

(*a*) (*b*)

The H_3 phase unit cell: (*a*) for $r = r_{10}$ and (*b*) in the interval $r_{10} < r < 1$.

ones, as shown in fig. 13 (*a*). The unit cell for this structure has hexagonal shape, thus we call this phase H_3. In order to be able to fit the cluster of small discs into the hexagon formed by the large ones, the diameter ratio r has to assume another 'magic' value, which we call r_{10}. This value is

$$r_{10} = 0{\cdot}386. \tag{15}$$

When the value of r increases beyond the 'magic' value r_{10}, we let the unit cell of H_3 expand uniformly as shown in fig. 13 (*b*).

On the other hand, if the diameter ratio becomes smaller than r_{10}, but is still higher than r_6 (the 'magic' value below which three small discs can be placed into an interstice of the pure A lattice), we have to distort the hexagonal unit cell, thus forming a periodic

Fig. 14

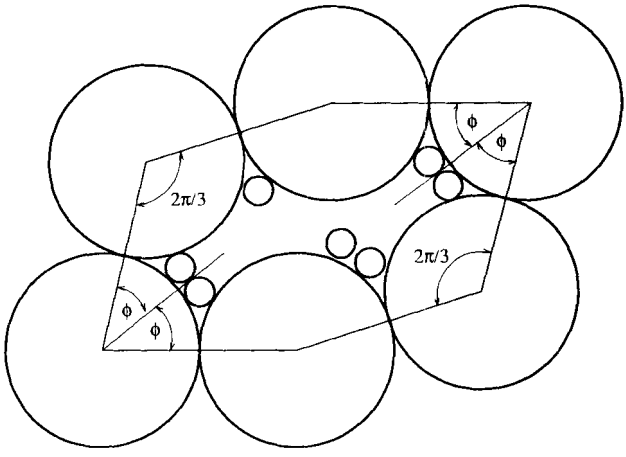

The H_3 phase unit cell for the A_2B_7 mixture in the interval $r_6 < r < r_{10}$.

structure with the unit cell shown in fig. 14. Referring to this fig., we note that each small disc in the lower left and upper right corners is in contact with the other small disc, and the two neighbouring large ones. As r approaches the value r_6, the H_3 phase evolves into a particular realization of the T_2^* 'lattice-gas' phase.

4.6. AB_8 *mixture* ($p = 8/9$)

We can start our search for candidate structures for this concentration, by trying to put four small discs into each of the interstices of the pure triangular A lattice. This can occur provided r does not exceed the 'magic' value

$$r_{11} = 0{\cdot}082, \tag{16}$$

where all small discs are in contact (with three small or one small and two large ones), as shown in fig. 15. We call the phase formed this way T_3.

When r becomes larger than r_{11}, we let the T_3 phase unit cell expand, so that the small discs still touch with small and large ones, but the large ones lose contact with each other. Thus, the unit cell takes shape shown in fig. 16 (*a*). However, this expansion cannot continue beyond the point where small discs from adjacent triangles touch. This occurs at the 'magic' value:

$$r_{12} = 0{\cdot}233, \tag{17}$$

and the unit cell looks as shown in fig. 16 (*b*). However, this phase never materializes, since its specific volume is slightly higher than that of the $A + B$ coexistence (see table 2).

4.7. *Mixtures with concentration* $p > 8/9$

From the results obtained in this section, it becomes clear that as the concentration of the small discs increases, there is a sequence of decreasing 'magic' radii for which we can exactly fit more and more small discs into the interstices of the triangular A lattice, this achieving maximum packing. We have calculated these magic radii for one, three and four small discs. Realizing that the phase diagram becomes arbitrarily complicated at higher concentrations, we do not examine structures with a number ratio larger than 8/9 (AB_8).

Fig. 15

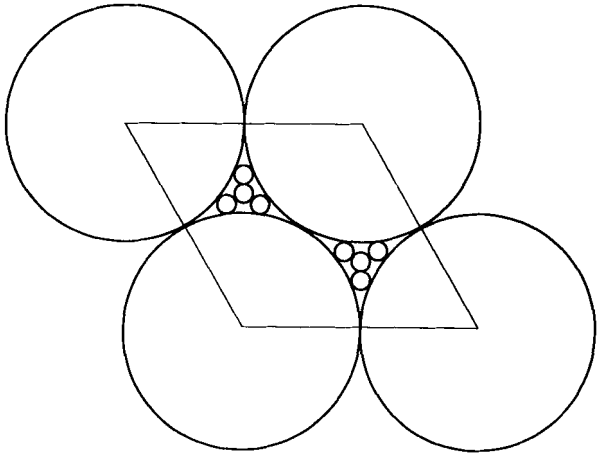

The T_3 phase unit cell for the AB_8 mixture at $r=r_{11}$.

Fig. 16

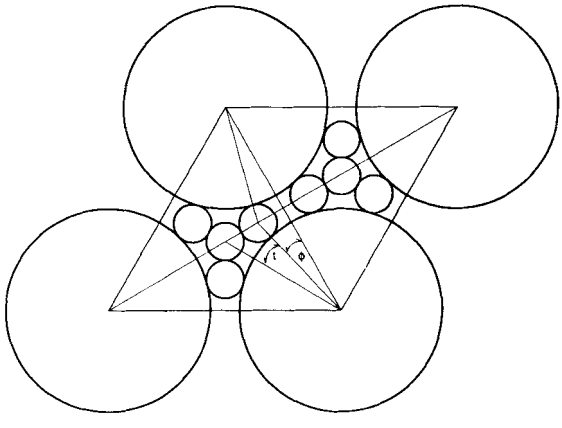

(*a*)

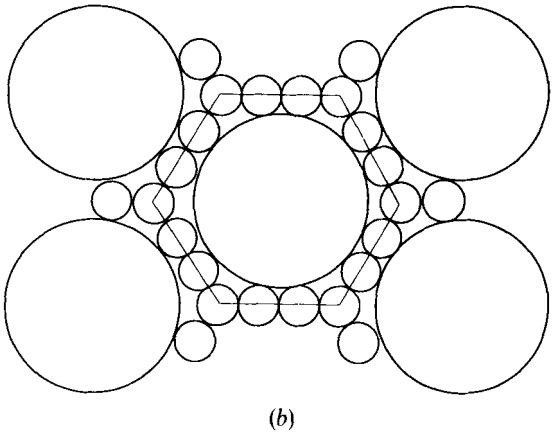

(*b*)

The T_3 phase unit cell for the AB_8 mixture: (*a*) in the interval $r_{11}<r<_{12}$ and (*b*) at $r=r_{12}$.

4.8. *'Lattice-gas' phases*

In §4.1, we found that for $r \leqslant r_1$ we could form AB_2 alloys by placing one small disc in each of the interstitial sites of the pure A triangular lattice, producing the T_1 phase. At the same interval for r, and for any mixture of the form $AB_{2-\delta}$ the interstices in the triangular A lattice outnumber the small discs which can, therefore, occupy any available site at random. The small discs, in effect, form a *lattice gas* on the honeycomb lattice formed by the interstices of the large discs. Thus, we call these phases $T_1^*(AB_{2-\delta})$, and refer to them as 'lattice-gas' phases. Clearly, they can be realized for all mixtures which are less rich in B than AB_2, when r is less or equal than r_1. The occupancy is thus $(2-\delta)/2$. In fig. 17, we show the unit cell of the $T_1^*(AB)$ phase, and in fig. 19 the unit cell of the $T_1^*(A_2B)$ phase (in both figs. the small discs occupying a particular site, so as to make the overall pattern periodic). As r approaches r_1 from above, the S_1 phase evolves into the particular *periodic* realization of $T_1^*(AB)$ shown in fig. 17.

The procedure can now be generalized to mixtures more rich in B than AB_2. Indeed, in §4.3 we produced the T_2 phase for the mixture AB_6 by putting a group of three B discs into each interstice of the A lattice. For all mixtures of the form AB_x with $2 < x < 6$, and for $r \leqslant r_6$, we can take away some of the small discs of the T_2 phase. As a consequence, some of the interstices of the A lattice will be occupied by three B discs, some by two some by one, and some others will be left unoccupied. This way, we generate another family of 'lattice gas' phases which we call $T_2^*(AB_{6-\delta})$ with $\delta < 4$. In figs. 19 and 20 we show particular realizations of the $T_2^*(AB_4)$ and $T_2^*(A_2B_7)$ phases respectively, which will make the overall pattern periodic. These are the realizations into which the S_2 and H_3 phases evolve, respectively, as r approaches r_6 from above.

It is now straightforward to think of the $T_3^*(AB_{8-\delta})$ 'lattice-gas' phases which will exist for mixtures of the form AB_x with $6 < x < 8$, and $r \leqslant r_{11}$, and so on. We show the region in which these phases occur in the phase diagram (fig. 24).

4.9. *'Random-tiling' phases*

For values of r exceeding r_1, we can form $AB_{2-\delta}$ structures by combining pure A triangles with the AB_2 unit cells. Examples are shown for the AB mixture in fig. 21 (*a*) for $r_1 < r < r_2$, and in fig. 21 (*b*) for $r > r_2$, and for the A_2B mixture in fig. 22 for $r_1 < r < r_2$. For values of r in the interval $r_1 < r < r_2$ the unit cell of the best AB_2 structure (fig. 4 (*a*)) was a rhombus with edge length unity—the same length as the edge of the equilateral triangle which makes up half the unit cell of the pure A phase. Consequently, we can fill

Fig. 17

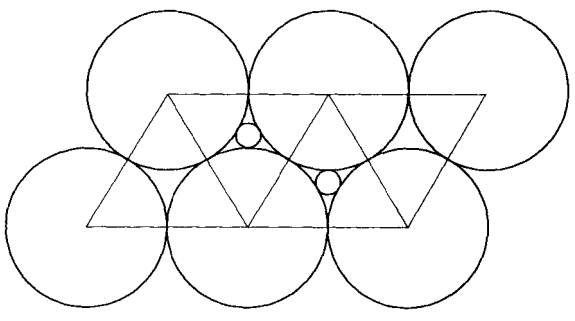

The T_1^* phase unit cell for AB mixtures at $r = r_1$.

Fig. 18

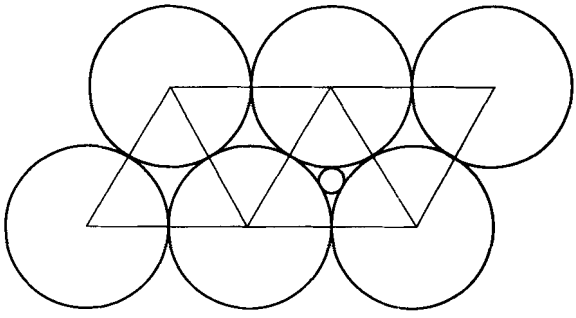

The T_1^* phase unit cell for A_2B mixtures at $r=r_1$.

Fig. 19

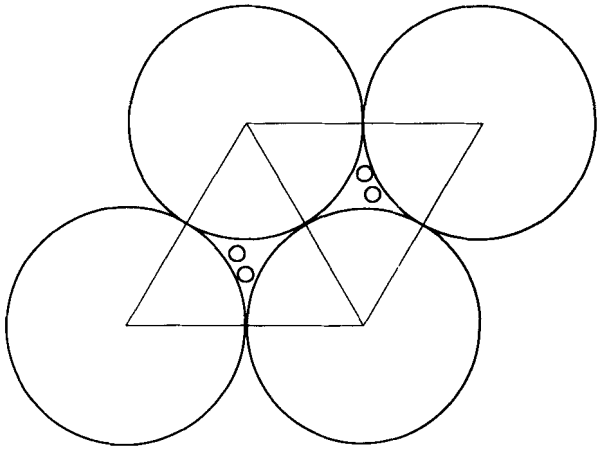

The T_2^* phase unit cell for AB_4 mixtures in the interval $0<r<r_6$.

Fig. 20

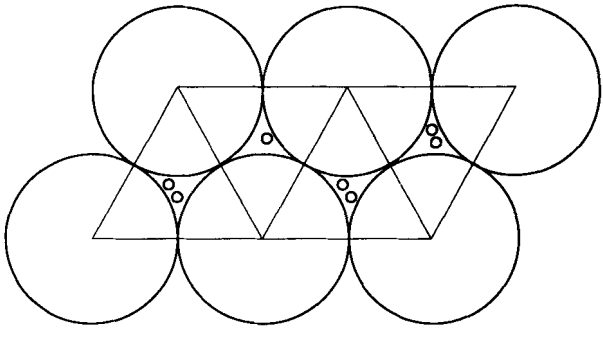

The T_2^* phase unit cell for the A_2B_7 mixture in the interval $0<r<r_6$.

Fig. 21

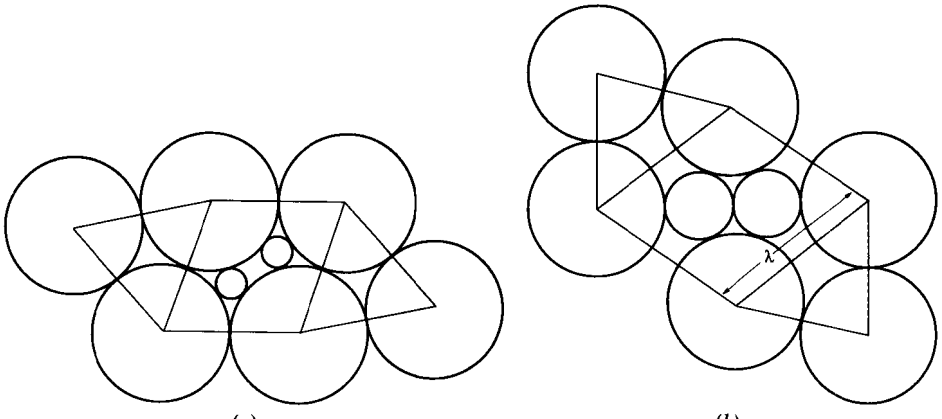

The $RT[(AB_2),(A)]$ phase unit cell for a periodic tiling of AB mixtures: (*a*) for $r_1 < r < r_2$ and (*b*) for $r > r_2$.

Fig. 22

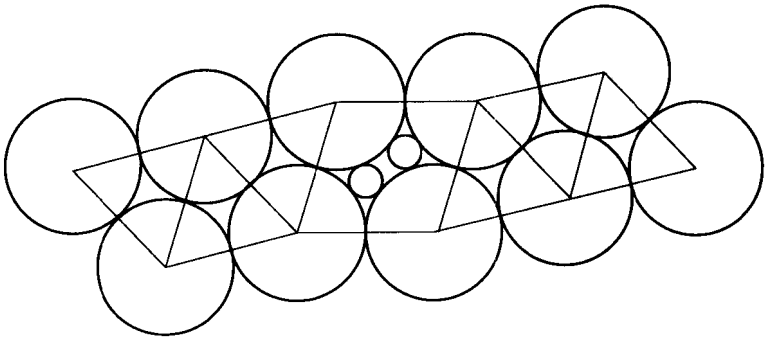

The $RT[(AB_2),(A)_3]$ phase unit cell for a periodic tiling of A_2B mixtures in the interval $r_1 < r < r_2$.

all space with *random tilings* of rhombi and triangles. Such tilings have only sixfold symmetry on average, but they are *topologically* equivalent to random tilings of squares and triangles which are known to be quasicrystals with 12 fold (dodecagonal) symmetry (Leung, Henley and Chester 1989, Widom 1993, Oxborrow and Henley 1993). For every square–triangle tiling, we choose one square and make an arbitrary choice between the two ways it can be sheared into a rhombus; having once made this twofold choice, the sense of shear is forced at every other square.

On the other hand, for the case $r > r_2$, we have a tiling of (AB_2) rhombi and of $(A)_{1/2}$ triangles, where the latter are now *isosceles* with long edge λ (fig. 21 (*b*)). It can easily be checked that the only possible tilings are combinations of 'strips' formed by AB_2 rhombi and A triangles. Each strip is bounded by straight rows of large discs; in the A strip discs of the two boundary rows are touching, while in the AB_2 strip they are separated by distances λ between large (A) discs. Thus, we can make a tiling consisting of any sequence of strips; the structure is random in one direction only, and the entropy per disc is zero in the thermodynamic limit. This is *not* a random tiling, according to the definition of Henley (1991).

Fig. 23

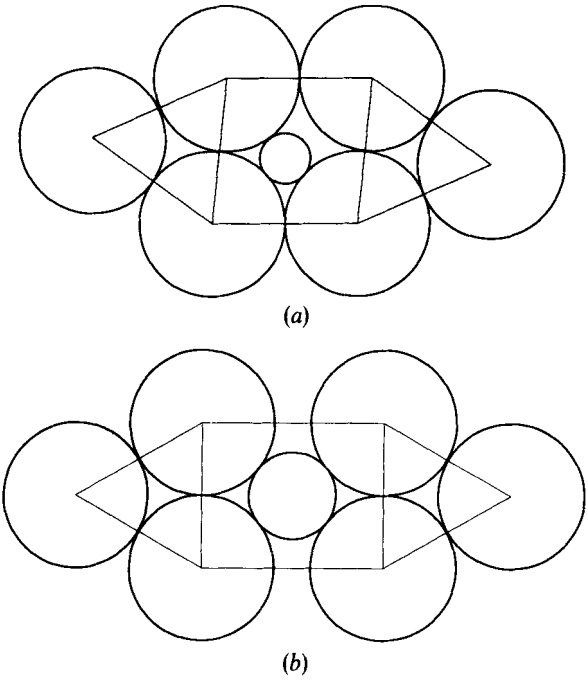

The $RT[(AB),(A)]$ phase unit cell for a periodic tiling of A_2B mixtures: (*a*) in the interval $r_1 < r < r_4$ and (*b*) in the interval $r_4 < r < 1$.

In both cases ($r_1 < r < r_2$ and $r_2 < r$), the 'average lattice' is incommensurate (Li, Park and Widom 1992) and can be described by projection from a space of $D = 3$ (modulation in one direction) or $D = 4$ (modulation in two directions). The 12 fold quasicrystal is a special case of $D = 4$. In figs. 21 (*a*, *b*) and 22, we show particular tilings which, if repeated throughout the plane, will result into a periodic structure. The formation of these phases is possible for all mixtures of the form $AB_{2-\delta}$, just by combining more and more $(A)_{1/2}$ triangles with the AB_2 unit cells. Accordingly, we call the phases generated this way $RT[(AB_2)_x, (A)_y]$, where x and y are chosen in such a way that the random-tiling phase has the appropriate concentration of B discs.

We can also combine $(A)_{1/2}$ triangles with the unit cell of the S_1 phase. This way we obtain another random tiling, called $RT[(AB)_x, (A)_y]$, which is possible for all mixtures of the form $AB_{1-\delta}$. At $r = r_4$ this is the square-triangle random tiling (Leung, Henley and Chester 1989). For a periodic tiling, and for $r_1 < r < r_4$, the $RT[(AB),(A)]$ phase for the A_2B mixture will have the unit cell shown in fig. 23 (*a*), whereas for $r_4 < r < 1$, it will have the unit cell shown in fig. 23 (*b*). For $r < r_4$, it is a rhombus–triangular tiling. For $r_4 < r$, it is a rectangle–triangle tiling. However, in the latter case, only a one-dimensional randomness is possible; the only tilings are combinations of 'strips' formed by AB rectangles and A triangles. The edges of the strips are straight rows of A discs in contact. Again, the entropy per disc of such tilings vanishes in the thermodynamic limit, and these are not random tilings according to the definition of Henley (1991)†.

† We repeat that the 'lattice gas' and 'random tiling' are both inherently random phases; they have a non-zero, discrete entropy per disc. The distinction is that, in the 'lattice gas' the *large* discs are in the *same* place in every one of the ensemble of close-packed configurations.

§ 5. The phase diagram

Having completed the first part of our search, which enabled us to make a selection among various candidate structures and reject the 'bad' ones, we can now proceed to the construction of the phase diagram in the (r, p) plane following the procedure outlined in § 3.1. The phase diagram is shown in fig. 24.

Not all the phases which have been found in § 4 to have the lowest specific volume survive the final competition. In § 4.9, we found that for all mixtures of the form AB_x with $x<2$, we can form 'random tiling' phases which we called $RT[(AB_2)_x,(A)_y]$ for $r>r_1$. We also found that in the interval $r_1<r<r_2$ these were true, *two-dimensional* random tilings having a non-zero configurational entropy per disc at the thermodynamic limit. These random tilings do survive, and appear in the phase diagram shown in fig. 24. However, in the interval $r>r_2$ they were one-dimensional 'pseudo-random tilings' whose entropy per disc vanished in the thermodynamic limit. The latter phases won the initial competition in small intervals above r_2 ($r_2<r<0{\cdot}299$ for the AB mixture and $r_2<r<0{\cdot}291$ for the A_2B mixture—see table 2). However, they get eliminated in the final competition in favour of the T_1+A coexistence. A similar situation occurs in the case of the $RT[(AB)_x,(A)_y]$ random tilings. These random tilings can occur for mixtures of the form AB_x with $x<1$. They are true, two-dimensional random tilings only in the interval $r_1<r<r_4$, and one-dimensional 'pseudo-random tilings' in the interval $r_4<r<1$. Although in the initial comparison the $RT[(AB),(A)]$ tiling won in the interval $0{\cdot}392<r<0{\cdot}436$ (see table 2), it is only in the interval $0{\cdot}392<r<r_4$ that it finally survives, because above r_4 it loses to the H_2+A coexistence. Thus, the only 'random-tiling' phases that appear in the phase diagram are true, two-dimensional random tilings.

A similar situation develops for some pure phases. In §§ 4.5, 4.6 we described the S_2 and H_3 pure phases, and as shown in table 2 it was found that the S_2 phase for the AB_4 mixture had the lowest specific volume in the intervals $r_6<r<0{\cdot}123$ and $0{\cdot}193<r<0{\cdot}245$. It is only in the latter interval, which lies around the 'magic' radius r_8

Fig. 24

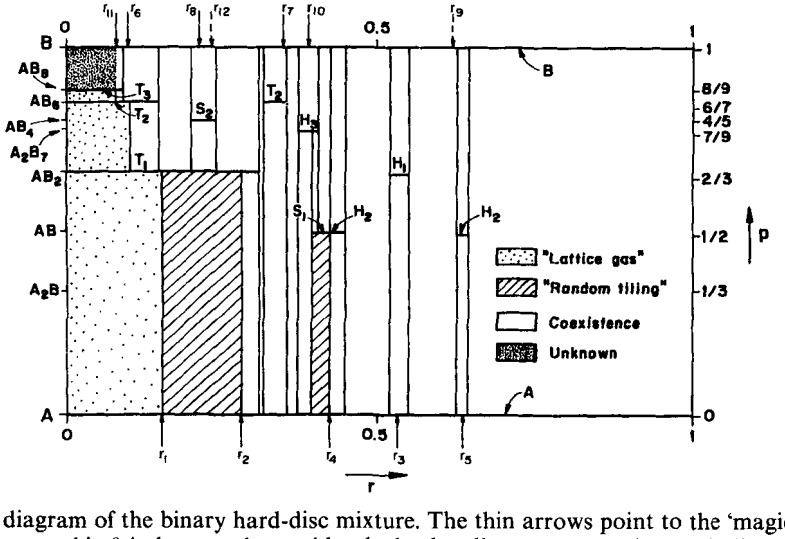

The phase diagram of the binary hard-disc mixture. The thin arrows point to the 'magic' radii discovered in § 4; the ones denoted by the broken lines correspond to periodic packings which never materialize.

that the S_2 phase finally survives, however; in the former interval, it gets eliminated in favour of the $T_2 + T_1$ coexistence. A similar situation occurs for the H_3 phase of the A_2B_7 mixture which does not survive in the interval $r_6 < r < 0{\cdot}110$, where the $T_2 + T_1$ coexistence prevails again, but only in the interval $0{\cdot}378 < r < 0{\cdot}408$, which again lies around the 'magic' radius r_{10} (see § 4.6). Trivially, the same is true for all the cases where the $A + B$ coexistence 'wins' over all other possible phases for a particlar concentration p, but for the same r there exists at least on other phase s which has 'won' for a different concentration p_s. Indeed, in that case the final result is $A + s$ coexistence for $p < p_s$ and $s + B$ coexistence for $p > p_s$.

In fig. 24, the heavy horizontal lines represent pure phases formed at specific values of the number ratio p, including the cases $p = 0$ (pure triangular A lattice) and $p = 1$ (pure triangular B lattice). The empty rectangles that are bounded above and below by the heavy horizontal lines represent the coexistence between the pure phases that bound them. The dotted regions represent the 'lattice-gas' phases, and the striped regions the 'random-tiling' phases. Finally, the heavily dotted region in the upper left corner represents the 'unknown' region which we did not study.

Referring to this figure, we observe that almost all of the complex alloy phases appear in the region $r \lesssim 0{\cdot}5$; the right-hand part of the phase diagram is dominated by the $A + B$ coexistence. There are two regions covered by 'random-tiling' phases, one for the $RT[(AB_2)_x, (A)_y]$, and one for the $RT[(AB)_x, (A)_y]$. The 'lattice-gas' phases at the left of the phase diagram form a '*staircase*' with decreasing width as the concentration p increases. The corners of the 'stairs' are the points $(r_1, 2/3)$, $(r_6, 6/7)$, and $(r_{11}, 8/9)$. Although we have not examined the 'unknown' region, it is clear from the discussion in § 4.7 that this 'staircase' will penetrate into the upper left corner with the width of the 'stairs' becoming smaller and smaller, probably in a self-similar way.

§ 6. Discussion

6.1. *Entropy effects*

As stated in § 3.1, the effects of entropy were ignored in all the calculations made thus far; that is we selected the 'winning' phases on the basis of minimization of specific volume (maximization of the packing fraction) *only*. In the cases of 'random' phases, there is a large number of structures which have the same volume V, and therefore (see eqn. (3)) are degenerate at $T = 0$. When $T > 0$, entropy makes certain of these structures more stable than the others. We discuss such effects below.

The first example are the 'lattice gas' phases. It is clear that the specific volume of the T_1^* phases is the same as that of the $T_1 + A$ coexistence. Similarly, the T_2^* phases have the same specific volume with the $T_2 + T_1$ coexistence, the T_3^* phases have the same volume with the $T_2 + T_3$ coexistence and so on. Thus, packing considerations alone do not 'prefer' one or the other. However, since the 'lattice gas' phases are all random phases, at finite temperatures there will be a non-zero, negative contribution to their free energy from an entropy of mixing 'particles' (B discs) with 'holes' (vacant interstices) in the underlying honeycomb lattice, and the random phases will be stabilized against the coexistence.

A similar situation exists for the 'random tiling' phases. Indeed, it can be easily seen that the $RT[(AB_2)_x, (A)_y]$ phases have the same packing fraction with the $T_2 + A$ coexistence, and the $RT[(AB)_x, (A)_y]$ phases have the same packing fraction as the $S_1 + A$ coexistence. Again, at $T > 0$ the free energy of the random phases will include a negative contribution from the entropy of mixing of rhombi with triangles, and they will prevail against the coexistence.

Finally, we should point out that there is yet another category of random phase, namely the substitutionally disordered triangular lattice, where large and small discs occupy the sites of a regular triangular lattice at random. Clearly, such a structure is always worse packed than the $A+B$ coexistence, and we did not need to consider it anywhere in our discussion. However, the disparity between the packing fraction of the disordered triangular structure and the $A+B$ separation becomes smaller and smaller as the size ratio r increases towards unity. On the other hand, the disordered phase has a non-zero mixing entropy per disc; thus we anticipate that at $T>0$ there will be a region of the phase diagram close to $r=1$ where, for all concentrations, the disordered triangular phase will become more stable than the $A+B$ coexistence. The three-dimensional analogue of this phase is the substitutionally disordered f.c.c. phase. This is indeed predicted to be stable at the freezing point for sufficiently large values of r, by density functional theories (Denton and Ashcroft 1990, Zeng and Oxtoby 1990).

6.2. *Extension to three dimensions*

We could apply the same systematics for guessing structures outlined in § 3.2 to consider candidate structures in three dimensions. In this fashion, we could obtain (at least) some well-known structures, such as the NaCl, CsCl, and the cubic Laves phases. If we try to fill interstices with small spheres (technique (i)), we will find that in three dimensions the interstitial holes are larger. If we consider the monodispersed simple cubic lattice as the 'parent structure', we find that the 'magic' radius for the CsCl structure, for example, is $r=\sqrt{3}-1$; however, the CsCl structure is always worse packed than the $A+B$ f.c.c.–f.c.c. coexistence. If we pursue technique (ii), substituting a single atom by a cluster, the most favourable case is surely that of an icosahedron, since it is much more spherical than, say a tetrahedron. This is the AB_{13} phase discussed by Sanders (1980) and Murray and Sanders (1980). Even in this case, the packing fraction is slightly worse than the $A+B$ coexistence (Murray and Sanders 1980). In contrast, for comparison, the 'two-dimensional analogue' of the AB_{13} phase, the H_3 phase, has a better packing than $A+B$ coexistence in the interval $0{\cdot}378<r<0{\cdot}408$ around its 'magic' radius r_{10} (see table 2).

It would appear that our techniques for guessing structures are less fruitful in three dimensions that in two dimensions. Indeed, we anticipate that the three-dimensional phase diagram of a binary mixture of hard spheres will be less rich than the two-dimensional one on general grounds. Three-dimensional structures have a larger coordination than two-dimensional ones (12 against 6 neighbours, in monatomic close-packed structures). Thus, to make 'magic' structures, we must typically satisfy too many simultaneous equations. In other words, distortions that close up vacant space and create contacts in certain directions, tend to make the packing worse in other directions, around a given atom. The assertion that the three-dimensional binary phase diagram will be less rich is also supported by the results of the earlier work by Murray and Sanders (1980). The difficulties with the packing could be addressed if a *third* species of spheres were present; so it may be necessary to study ternaries in three dimensions. Ternaries also appear to be particularly relevant to the study of quasicrystals (see below).

6.3. *Relevance to quasicrystals*

In the field of quasicrystals, since the detailed local arrangement of atoms is not established, hypothetical atomic arrangements are constructed and tested for local stability using pair potentials. The *monatomic* patterns which are locally stable under

short-range potentials (Roth, Schilling and Trebin 1990) tend to be the same as the good sphere packings (Henley 1986).

The alloy systems in which quasicrystals occur tend to have complicated phase diagrams including a number of ordered alloys with large unit cells. In the real materials, interactions with distant neighbours (from the Friedel oscillations in the effective potentials obtained by integrating out conduction electrons) and angle-dependent (many-atom) terms are undoubtedly important. Still, one would like to understand whether this complicated behaviour *requires* complicated interactions, or whether it can be obtained with the simplest ones, i.e. hard spheres (or discs). Therefore, it is very useful to have toy models to describe quasicrystals, in somewhat the same way that the hard spheres serve as a toy model for f.c.c. crystals.

One of our models is indeed a quasicrystal: namely, the case $r=\sqrt{2}-1$ and $p=(3-\sqrt{3})/4$ (Leung *et al.* 1989). For this value of r, the ideal close packing would be a coexistence of domains of all squares (AB) and domains of all triangles (A). Both structures have lattice constants of unity, so that boundaries between squares and triangles can cost nothing, and furthermore the corner angles $\pi/4$ and $\pi/6$ are rationally related. The squares dissolve into the triangles, so that any random square-tiling has an equally good packing. This ensemble, which has a non-zero discrete configurational entropy per atom, has been shown to be a random-tiling quasicrystal (Kawamura 1991, Oxborrow and Henley 1993, Widom 1993). In other words, an *average* over all allowed configurations has 'quasi-long-range-order' (i.e. algebraic diffraction peaks) at the Bragg points of a 12 fold symmetric quasi-periodic structure.†

Another toy model of quasicrystal is the 'binary tiling', a binary system of large and small atoms with non-additive interaction radii. This has always been formulated in terms of soft (usually Lennard-Jones) potentials, although it would surely give the best packing for non-additive hard constraints. Again, the ground state is a random tiling quasicrystal, this time with tenfold symmetry (Lançon, Billard and Chaudhari 1986, Widom, Strandburg and Swendsen 1987).

In three dimensions a random-tiling quasicrystal would have true Bragg peaks. It would be highly desirable to have a toy model generalizing the 'binary tiling' to three dimensions, in terms of interacting particles, such that the ground states correspond to icosahedral tiling configurations. The simplest kind of interaction is a hard-sphere constraint. As we argued in § 6.2, we expect the three-dimensional phase diagram of a binary hard-sphere alloy to be less complicated than the two-dimensional hard-disc phase diagram. However, it is sometimes suggested that the third species (e.g. Si in AlMnSi or TiMnSi) is needed in order to fit into the 'smaller' sites, i.e. the size ratios are the essential ingredient in the stabilization which is found at a special concentration. It may, therefore, be necessary to investigate ternaries before a suitable model can be found; it is particularly intriguing that good quasicrystals are all ternaries (e.g. AlCuLi, AlCuFe, AlPdMn).

§ 7. Conclusions

We wished to explore how complicated the generic shape of an alloy phase diagram might be, and how complicated the atomic structures might be. For this purpose, we

† A Lennard-Jones version of this system was simulated (Leung *et al.* 1989) but the hard-disc system has never been simulated: since its packing fraction is only about 1% better than phase separation into A and B triangular lattices, it was anticipated that it would be difficult to equilibrate.

chose hard discs as a toy model. We anticipate that if we were to use realistic potentials ('realistic' would be hard to define in two dimensions!) we would find the same candidate phases as were constructed in § 4; however, their ranges of stability might be quite different. The most important precondition for making a realistic atomic structure (for short-ranged potentials) is that (i) there should be no excessively close atoms and (ii) there should be no large vacant volumes. Obviously, any structure with an optimal packing fraction will satisfy these conditions, although the converse is not necessarily true. Our result is non-rigorous, in that we have considered only a selected, finite set of structures. Nevertheless, we suspect that our phase diagram is accurate, since we have considered many structures that ultimately did not appear in the phase diagram at all.

We discovered about ten moderately complicated alloy phases, most of them in the region $r \lesssim 0{\cdot}5$. Large regions of the phase diagram are occupied by random phases, i.e. the 'lattice gas' and 'random tiling' phases. The phase diagram becomes arbitrarily complicated as the concentration of small discs increases toward unity and the size ratio becomes increasingly small.

Acknowledgments

We wish to thank Dr R. Phillips for a careful reading of the manuscript and useful comments, and Professor N. W. Ashcroft for helpful discussions. This work was supported by the Materials Science Center at Cornell University, under Grant No DMR-9017281 and the Department of Energy, Grant No DE-FG02-89ER-45405.

References

Ashcroft, N. W., 1982, Dense Conducting Fluids, *The Liquid State of Matter: Fluids, Simple and Complex*, edited by E. W. Montroll and J. L. Lebowitz (Amsterdam: North Holland), pp. 141–175.

Ashcroft, N. W., and Mermin, N. D., 1976, *Solid State Physics*, (Philadelphia: Holt-Saunders), chap. 19.

Bartlett, P., 1990, *J. Phys: Condens. Matter*, **2**, 4979.

Bartlett, P., and Ottewill, R. H., 1991, *J. chem. Phys.*, **96**, 3306.

Bartlett, P., Ottewill, R. H., and Pusey, P. N., 1990, *J. chem. Phys.*, **93**, 1299; 1992, *Phys. Rev. Lett.*, **68**, 3801.

Bideau, D., Gervois, A., Oger, L., and Troadec, J. P., 1986, *J. Phys., Paris*, **47**, 1697.

Denton, A. R., and Ashcroft, N. W., 1990, *Phys. Rev.* A, **42**, 7312.

Dodds, J. A., 1975, *Nature*, **256**, 187.

Fejes Toth, L., 1964, *Regular Figures*, (New York: Macmillan), p. 153; 1972, *Lagerungen in der Ebene auf der Kugel und im Raum*, (Berlin: Springer-Verlag), p. 73.

Henley, C. L., 1986, *Phys. Rev.* B, **34**, 797; 1991, Random Tiling Models, *Quasicrystals: The State of The Art*, edited by P. J. Steinhardt and D. P. DiVincenzo, (Singapore: World Scientific), chap. 15; section 3.

Kawamura, H., 1991, *Physica* A, **177**, 73.

Lançon, F., Billard, L., and Chaudhari, P., 1986, *Europhys. Lett.*, **2**, 625.

Leung, P. W., Henley, C. L., and Chester, G. V., 1989, *Phys. Rev.* B, **39**, 446.

Li, W., Park, H., and Widom, M., 1992, *J. statist. Phys.*, **66**, 1.

Murray, M. J., and Sanders, J. V., 1980, *Phil. Mag.* A, **42**, 721.

Nowick, A. S., and Mader, S. R., 1965, *IBM J.*, Sept.–Nov., p. 358.

Oxborrow, M., and Henley, C. L., 1993, *Phys. Rev.* B, (to be published).

Pauling, L., 1960, *The Nature of the Chemical Bond* (Ithaca, N.Y.: Cornell University Press), p. 523.

Quickenden, T. I., and Tan, G. K., 1974, *J. Colloid. Sci.*, **48**, 382.

RICK, S. W., and HAYMET, A. D. J., 1989, *J. chem. Phys.*, **90,** 1188.
ROTH, J., SCHILLING, R., and TREBIN, H.-R., 1990, *Phys. Rev.* B, **41,** 2735.
SANDERS, J. V., 1980, *Phil. Mag.* A, **42,** 705.
SZETO, K. Y., and VILLAIN, J., 1987, *Phys. Rev.* B, **36,** 4715.
VILLAIN, J., SZETO, K. Y., MINCHAU, B., and RENZ, W., 1988, Dense packings of hard spheres, *Competing Interactions and Microstructures: Statics and Dynamics*, edited by R. LeSar, A. Bishop and R. Heffner, (Berlin: Springer-Verlag), p. 128–38.
VISSCHER, W. M., and BOLSTERLI, M., 1972, *Nature*, **239,** 504.
WIDOM, M., 1993, *Phys. Rev. Lett.*, **70,** 2094.
WIDOM, M., STRANDBURG, K. J., and SWENDSEN, R. H., 1987, *Phys. Rev. Lett.*, **58,** 706.
ZENG, X. C., and OXTOBY, D., 1990, *J. chem. Phys.*, **93,** 4357.